European Journal of Pharmaceutics and Biopharmaceutics 77 (2011) 283–296

Contents lists available at ScienceDirect

European Journal of Pharmaceutics and Biopharmaceutics

journal homepage: www.elsevier.com/locate/ejpb

Research paper

The production of 'aerodynamically equivalent' drug and excipient inhalable powders using a novel fractionation technique

Mohammed Taki [a,*], Christopher Marriott [a], Xian-Ming Zeng [b], Gary P. Martin [a]

[a] King's College London, Institute of Pharmaceutical Science, London, United Kingdom
[b] TEVA Pharmaceuticals, Global Respiratory R&D, Miami, USA

ARTICLE INFO

Article history:
Received 9 August 2010
Accepted in revised form 20 November 2010
Available online 23 December 2010

Keywords:
Particle size distribution
Aerodynamic fractionation
Salmeterol xinafoate
Fluticasone propionate
Aerodynamically equivalent powders

ABSTRACT

Inhalation particles can be produced by various techniques such as milling, controlled crystallisation and spray-drying, but current methods cannot, to-date, precisely control the aerodynamic size distribution of produced powders. The aim of this study was to develop and validate a novel preparative technique whereby the efficient and reproducible aerodynamic fractionation of drug and excipient powders could be achieved. Salmeterol xinafoate (SX), fluticasone propionate (FP) and fine α-lactose monohydrate (FL) were chosen as model compounds. Powders were aerosolised using a dry powder feeder into a Next Generation Impactor operated at 60 L min^{-1}. Powders deposited on NGI stages were then collected and analysed. The fractionation process was successful for all powders producing significant linear correlations between the pre-set aerodynamic cut-off limits and geometric size measurements. For each of SX, FP and FL, sufficient powder quantities were recovered from NGI stages 1–6 producing six fractions with sequential aerodynamic and geometric particle size distributions. The fractionation technique was efficient and reproducible for all powders studied. The method can be equally applied to various drugs and excipients regardless of their previous production/processing history. Therefore, the aerodynamic fractionation technique may be used to compare and contrast samples produced by different processes.

1. Introduction

Inhaled particles, which are typically required to have a mass median aerodynamic diameter (MMAD) of <5 μm, can be produced by the milling of larger particles, spray-drying the compound of interest from a liquid or crystallisation from a solvent using a variety of techniques. Fluid energy milling or 'micronisation' is commonly used whereby jets of compressed air – usually two jets positioned in a horizontally opposing manner – carry the solid particles forcing them to impact with one another at high speeds leading to attrition and a consequent reduction in particle size. A particle size classifier is incorporated in the system, typically in the shape of a cyclone, to ensure the exclusive removal of particles having a sufficiently small size. Large amounts of energy are required to produce particles in the size range suitable for deep lung delivery. The violent nature of the process often leads to the production of particles that possess high surface energy and electrostatic charge [1]. Additionally, solid-state transformation can be introduced by this high energy milling process leading to amorphism especially at the particle surface [2,3]. Despite these disadvantages, milling continues to be the most widely employed technique for the production of 'respirable' particles [4].

Spray-drying has been routinely employed for the production of pharmaceutical particles for decades [5]. The compound is fed as a solution or suspension in a liquid medium and atomised into a hot drying environment. Particles produced by spray-drying are usually amorphous, more spherical and possess a lower density compared to milled particles [6]. Amorphous particles produced by spray-drying have been shown to revert to a more crystalline state when exposed to elevated temperatures and/or humidity. Such transformations can lead to significant differences in the physicochemical properties of the powder resulting in changes to particle deposition following aerosolisation (aerodynamic deposition) [7].

A variety of crystallisation techniques have also been employed in the production of micron-sized particles. Anti-solvent crystallisation strategies involving the use of conventional solvents have been widely reported [8–11]. Supercritical fluids have also been successfully employed for the production of fine particles in sizes suitable for inhalation [12–15]. Crystallisation techniques have the advantage of producing particles of high crystallinity and hence higher inherent physical stability.

The three fine particle production methods discussed: milling, spray-drying and crystallisation, differ in their principles of operation leading to a contrasting set of advantages and disadvantages in the

* Corresponding author. King's College London, Institute of Pharmaceutical Science, 150 Stamford Street, London SE1 9NH, United Kingdom. Tel.: +44 (0) 7734219194; fax: +44 (0)207 848 4800.
E-mail address: mohammed.taki@kcl.ac.uk (M. Taki).

0939-6411/$ - see front matter © 2010 Elsevier B.V. All rights reserved.
doi:10.1016/j.ejpb.2010.11.021

resultant particles. However, all three methods – to-date – lack the ability to produce particles of a precisely controlled aerodynamic size distribution. With all three methods, particles are produced *then* their size is determined using a particle size measurement method, typically a light-scattering-based one. The particle size distribution is, therefore, usually regarded to be suitable according to the geometric – rather than the aerodynamic – size of the particle. The parameters of the powder production process are then set on the basis of the measured particle size. The aerodynamic size of the drug particles is then usually determined following a formulation process which itself might influence the aerodynamic size measured. It is typically difficult with all micron-sized-particle production methods to precisely and reproducibly regulate the geometric particle size distribution. This is attempted by tight control of the production process parameters, but there are often difficulties in achieving a narrow-distribution of the 'desired' particle size.

Nevertheless, it is the aerodynamic particle size distribution of a powder that is widely accepted as the key parameter ultimately determining lung deposition [15–19]. It is difficult to predict impactor penetration and lung deposition from geometric measurements alone since the aerodynamic particle size takes into consideration the particle's geometric size, shape and density. In order to study the significance of physico-chemical factors other than particle size in determining the aerodynamic deposition of a particle on an impactor stage *in vitro* and in the airways *in vivo*, samples should ideally possess a similar aerodynamic particle size such that any differences observed in aerodynamic deposition can be attributed to other variables. Considering the fine particle production techniques discussed above, it is difficult to use any of these to produce samples having an 'equivalent' geometric size from different drugs or excipients let alone samples having an 'equivalent' aerodynamic size distribution. Should a technique be developed that can produce samples from different actives and/or excipients having 'equivalent' aerodynamic diameters then it may prove to be a useful research tool. The method should largely be unaffected by the physico-chemical properties of the sample while producing comparable and reproducible particle size distributions. Additionally, the method should allow for the aerodynamic particle sizing of samples *prior* to mixing with other drugs and/or excipients which enables the undertaking of simple direct comparisons between multiple powders.

Impactors, such as the next generation impactor (NGI), have been designed for the analytical fractionation of powders on basis of the particles' aerodynamic sizes. The operation of an impactor is largely unaffected by the physico-chemical nature of the fine powder. However, fine drug particles are usually mixed with coarse carrier particles possibly in the presence of fine excipient particles in an attempt to overcome, to some extent, the cohesive forces that typically dominate fine particle interactions. Therefore, any aerodynamic sizing technique that is utilised should ensure that drug agglomerates are sufficiently de-agglomerated prior to impactor fractionation.

The aim of this study was to seek to develop and validate a novel preparative technique whereby the efficient and reproducible aerodynamic fractionation of drug and excipient powders could be achieved using the Next Generation Impactor.

Salmeterol xinafoate (SX) and fluticasone propionate (FP) were chosen as two model drugs for fractionation since the presence of these two different active ingredients in a combination formulation may enable the investigation into how different drug entities perform aerodynamically under identical conditions. In addition, fine lactose (FL) is often included as an excipient in DPI formulations and the production of FL fractions that are 'aerodynamically equivalent' to drug samples may prove very useful in the production of control formulations as well as the undertaking of studies into drug-excipient interactions.

2. Materials and methods

2.1. The production of micron-sized particles

SX (Vamsi Labs Ltd., Maharashtra, India) was micronised using a Trost GEM-T microniser (Plastomer Technologies, Houston, USA) connected to a supply of compressed air via a valve and a pressure gauge with the 'O' and 'P' jet pressures maintained at 40 and 60 psi, respectively. The micronised powder was collected from the mill's collection jar. The Malvern Mastersizer was employed to determine the volume-weighted particle size distribution of the unmicronised FP sample (Coral Drugs Ltd., New Delhi, India). The particle size distribution of FP was found to broadly comprise a size range suitable for inhalation. The original solvent-crystallised, unmicronised FP powder was therefore used for fractionation. Fine α-lactose monohydrate (Lactohale 300, Friesland Foods Domo Ltd., Chester, UK) was received as a milled sample with a reported median particle size of 5 μm. A similar size was obtained using the Malvern Mastersizer, and consequently, fine lactose (FL) was used without further milling.

2.2. Aerodynamic fractionation of powders using the NGI

2.2.1. Powder aerosolisation

SX, FP and FL were aerosolised using a Malvern QSpec dry powder feeder (Malvern Instruments Ltd., Worcestershire, UK) as shown in Fig. 1. The jet pressure of the dry powder feeder (DPF) was set midway between dial marks 2 and 3 producing a nominal jet pressure of 1 bar. The resultant airflow rate at the DPF outlet was approximately 50 L min^{-1}. The feed rate was set at dial marks 4–7 depending on a visual estimate of the actual amount of powder being aerosolised ensuring that the amount was sufficient but not so great as to overload the NGI. The DPF was placed on a lab jack, and the height was adjusted such that the outlet of the DPF was in-line with the centre of the NGI throat both vertically and horizontally. The DPF was connected to a supply of compressed air and vacuum via the appropriate ports using vacuum tubing (internal diameter = 5 mm). Particle density was measured using a helium AccuPyc 1330 pycnometer (Micromeritics, Dunstable, UK). The instrument was calibrated prior to testing as outlined by the manufacturer. Each sample was analysed six times, at a helium purge pressure of 14.5 psi.

2.2.2. Powder fractionation and recovery

The NGI pre-separator was filled with 15 mL of filtered dispersant (see below). The NGI was assembled, connected to a vacuum pump, and the flow rate, measured at the air inlet (throat), was adjusted to 60 L min^{-1} using a flow-control valve positioned between the NGI air outlet port and the vacuum pump. The calculated NGI stage cut-off diameters at a flow rate of 60 L min^{-1} are shown in Table 1. The NGI cups were labelled 'S1', 'S2', 'S3', 'S4', 'S5', 'S6', 'S7' and 'MOC', as appropriate, and were used uncoated. An amount of 2.0 g of powder was placed on the feeding tray of the DPF, the feeder was switched on, the 'airflow' dial was set to 'airflow' and the flow rate was allowed to stabilise for 1 min. The vacuum pump connected to the NGI was then started and the DPF 'airflow' dial switched to 'feed' simultaneously for a period of 20 s. The vacuum pump was then switched off and the DPF 'airflow' dial changed back to 'airflow'. Powder deposits on each NGI cup (Fig. 2) were transferred onto clean, labelled sheets of paper with the aid of a spatula. Each NGI cup was then replaced in its position as labelled, the NGI re-assembled and the vacuum pump and the powder feed restarted as described above. This procedure was repeated until the DPF feeding tray was empty. Powders were then transferred from the labelled sheets into sealed glass vials and stored in a

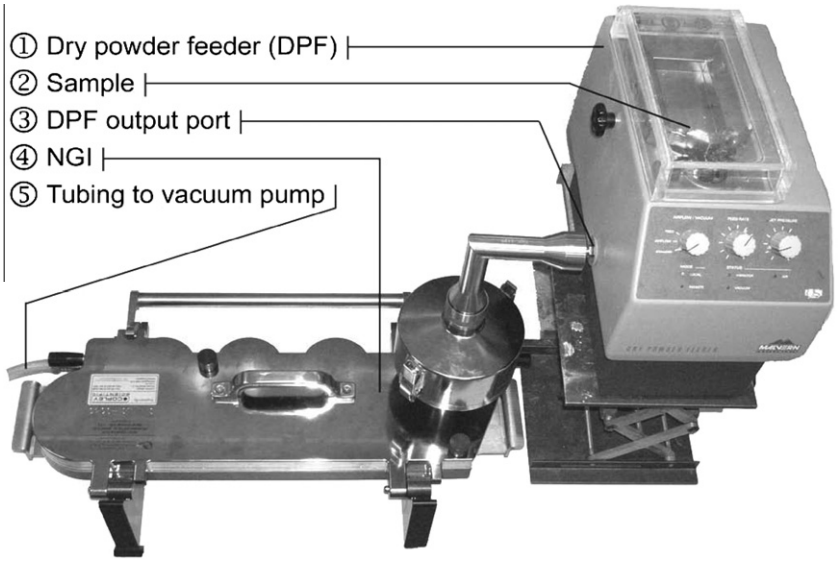

Fig. 1. The experimental arrangement employed for the aerosolisation of SX, FP and FL powders using the Malvern dry powder feeder for fractionation by the NGI.

Table 1
Calculated cut-off diameters (μm) of NGI stages at a flow rate of 60 L min^{-1}.

NGI stage	Cut-off diameter at 60 L min^{-1} (μm)
Pre-separator	12.8
1	8.06
2	4.46
3	2.82
4	1.66
5	0.94
6	0.55
7	0.34

desiccator containing silica gel (Prolabo, VWR International, UK) until required. The fractionation process was performed in triplicate for each of SX, FP and FL.

2.3. Measurement of particle size using a light-scattering-based technique

The geometric particle size distribution of samples was determined by light-scattering using a Malvern Mastersizer X (Malvern Instruments Ltd., Worcestershire, UK) equipped with a 100-mm focal length lens (measurement range: 0.5–180 μm) and an MS7 magnetically stirred cell. The active laser beam length was 14.3 mm. SX, FP and α-lactose monohydrate (FL) samples were dispersed in filtered saturated solutions prior to particle size measurement. SX and FP were dispersed in SX- and FP-saturated 0.5% (w/v) Span 80 in cyclohexane solutions, respectively, while lactose was dispersed in a lactose-saturated propan-2-ol solution. Span 80 (sorbitan monooleate) was obtained from Sigma–Aldrich Company Ltd. (Dorset, UK), while cyclohexane and propan-2-ol (both HPLC grade) were obtained from Thermo Fisher Scientific Inc. (Loughborough, UK). SX, FP and lactose-saturated solutions were prepared by ultra-sonicating excess amounts of each compound in the relevant dispersant for 2 h. Dispersants were then stirred by means of a magnetic follower at room temperature over night. Amounts were removed from these stock solutions, as required, by means of a glass-syringe and filtered using 0.20-μm cellulose acetate syringe filters (Orange Scientific, Belgium).

Samples were prepared for measurement by placing approximately 1 mg of powder in an 8-mL glass vial and adding 3 mL of filtered dispersant. The suspension was homogenously dispersed by placing the glass vial in an ultrasonic water bath (Sonicleaner, Dawe Ultrasonics Ltd., USA) for 3 min followed by vigorous shaking for 10 s. Filtered dispersant (approximately 15 mL) was added to the magnetically stirred sample cell with the stirrer speed set at four scale units. A sample of dispersed suspension was then added by means of a Gilson pipette until an obscuration of approximately 20% (±2%) was achieved. Samples were allowed an equilibration time of 60 s before the first analysis was performed. Each sample was scanned five times each consisting of 2500 sweeps. Three samples were analysed from each powder ensuring a different location in the powder bed was used each time.

The light-scattering patterns of SX, FP and FL were analysed in accordance with the Lorenz-Mie theory using the software provided with the Mastersizer machine (version 2.19). The 'real'

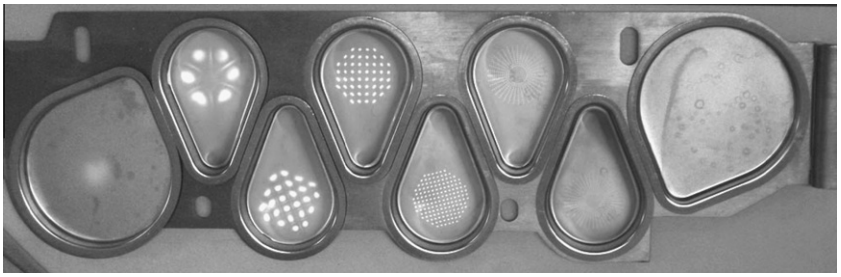

Fig. 2. NGI tray with collection cups containing lactose deposits. Stage 1 collection cup is shown on the left.

refractive index values used for SX and FP were 1.623 and 1.570, respectively, [20] while a 'real' refractive index value of 1.533 was used for lactose [21]. The 'imaginary' component of the refractive index used for SX, FP and FL was 0.1. The refractive indices of cyclohexane and propan-2-ol were taken as 1.426 and 1.378, respectively.

2.4. Scanning electron microscopy (SEM) of fractions

A small amount of each sample was transferred using a spatula onto a glass cover slip which had been adhered to an SEM aluminium stub using double-sided adhesive tape. The stub was then gently tilted and rotated while being tapped using a spatula causing the powder to form a thin layer and any excess to be removed. The powder-containing SEM stubs were then sputter coated with gold using a Polaron E51000 gold coating machine (Polaron Equipment Ltd., Quorum Technologies, Newhaven, UK). The thickness of the gold layer was approximately 15 nm. Electron microscopy was carried out using an FEI Quanta 200F field emission environmental scanning electron microscope (FEI Company, Eindhoven, The Netherlands). SEM analysis was performed under high vacuum using a beam-voltage of 5.0 kV and an ETD detector from a working distance of 10–15 mm.

2.5. Data analysis

The stage cut-off diameter at a flow rate of 60 L min^{-1} of the NGI stage at which the powder was deposited together with the cut-off of the preceding stage was used to calculate the geometric mid-range values (denoted herein as M) given by:

$$\text{cut-off mid-range } (M_n) = \sqrt{\text{stage}_n \times \text{stage}_{n-1}} \quad (1)$$

where (n) and $(n-1)$ are the numbers of the stage on which the powder is collected and the stage preceding it, respectively. For deposits on stage 1, the cut-off diameters of stage 1 and the pre-separator, 8.06 μm and 12.8 μm, respectively, were used producing a cut-off mid-range value of 10.16 μm.

$D(v,0.5)$ is the median particle equivalent diameter in the volume distribution while $D(v,0.1)$ and $D(v,0.9)$ are the 10th and 90th percentiles, respectively, of the cumulative volume-based distribution of particle equivalent diameters. The mode diameters [D(mode)] reported represent the mode having the highest frequency in cases where more than one mode was present.

The spread of particle diameters is given by the 'span' where:

$$\text{span} = \frac{d(v,0.9) - d(v,0.1)}{d(v,0.5)} \quad (2)$$

3. Results

3.1. Micronisation results

SX was successfully micronised producing a sample having a median particle size of 2.67 μm from the original powder which had a median size of 11.99 μm (Table 2).

When micronised SX was fed into the micronizer, a smaller particle size was obtained initially, but this double-micronised sample was unstable and a large second particle size mode of 9.25 μm appeared in light-scattering-based particle size measurements upon storage for approximately 1 week. The suppliers of FL (Friesland Foods Domo Ltd., Chester, UK) claimed that the Lactohale 300 sample used had $D(v,0.1)$, $D(v,0.5)$ and $D(v,0.9)$ values of 3.0, 5.0 and 8.0 μm, respectively. However, the median particle size of FL was found to be <5 μm (Table 2). Despite the apparent difference in these values, both sets of data confirmed the sample to be of a suitable 'respirable' particle size. FL was, therefore, used in the fractionation process as supplied without further particle size reduction.

Table 2
Particle sizes (μm) of original unmicronised SX (Orig. SX), micronised SX (MSX), original unmicronised FP (Orig. FP) and FL as supplied. The data determined by light-scattering corresponding to 10th, median and 90th percentile particle volume-equivalent diameter [mean values ± SD (n = 3)].

Sample	$D(v,0.1)$	$D(v,0.5)$	$D(v,0.9)$	D(mode)	Span
Orig. SX	3.2 ± 0.4	12.0 ± 0.7	28.6 ± 1.5	15.7 ± 1.0	2.1 ± 0.0
MSX	0.9 ± 0.1	2.7 ± 0.3	6.9 ± 0.6	2.7 ± 0.2	2.3 ± 0.2
Orig. FP	1.0 ± 0.3	4.1 ± 0.3	11.2 ± 0.5	4.3 ± 0.2	2.5 ± 0.1
FL	0.9 ± 0.2	3.5 ± 0.1	8.9 ± 0.4	3.9 ± 0.1	2.3 ± 0.1

3.2. Deposition per NGI stage

The quantity of powder deposited on a given NGI stage varied considerably between the different compounds (Table 3). However, similar trends of relative deposition on the different stages were observed with all compounds. For the three powders, the greatest amount of deposition was achieved on stage 4 followed by stages 3 and 2, respectively. More was typically deposited on stage 5 than stage 1 for SX and FL while the reverse was obtained with FP. Very small amounts were deposited on stages 7 and MOC for all three compounds rendering it difficult to obtain a sufficient sample size for full analysis. Out of the total 6 g aerosolised in each case, the percentage mean recovery was 74%, 68% and 75% for SX, FP and FL, respectively. The remainders in each case constitute deposits in the pre-separator as well as powder losses which occurred during the experiment.

3.3. The aerodynamic fractionation of SX

The particle sizes of SX fractions recovered from NGI stages 1–6, respectively, were sequentially smaller (Table 4 and Fig. 3). Deposits on stage 1 produced a geometric volume-equivalent median particle size of 8.96 μm while particles recovered from stage 6 had a median size of 1.28 μm. $D(v,0.1)$ and $D(v,0.9)$ values also decreased successively for powders deposited on stages 1–6, respectively. The micronised SX (MSX) powder used to produce the fractions had a pre-fractionation median size of 2.67 μm. When comparing the geometric median size obtained from each NGI stage, all fractions were significantly different (ANOVA, $p < 0.05$). In addition, fractions had a significantly smaller spread in particle size compared to the pre-fractionation MSX powder, as indicated by their lower span values (ANOVA, $p < 0.01$; Table 4). Plots of geometric median diameter and D(mode) against stage cut-off mid-range values (M) produced linear relationships with correlation co-efficient (r^2) values of 0.985 and 0.975, respectively (Fig. 5). Both correlations were statistically significant ($p < 0.0001$).

Table 3
Mean amount (±SD) of powder collected on each NGI stage following aerosolisation using the DPF (n = 3). The total amount aerosolised in each run was 2.0 g.

NGI stage	Amount (mg)		
	SX	FP	FL
Stage 1	98.0 ± 18.2	135.3 ± 22.9	97.4 ± 13.2
Stage 2	228.8 ± 36.3	236.8 ± 37.0	245.5 ± 39.2
Stage 3	392.2 ± 60.0	338.3 ± 54.8	401.1 ± 78.1
Stage 4	553.6 ± 100.7	441.3 ± 82.7	544.6 ± 99.2
Stage 5	130.7 ± 21.7	121.8 ± 21.7	145.5 ± 37.1
Stage 6	65.4 ± 14.2	81.2 ± 12.2	55.4 ± 10.2
Stage 7	4.9 ± 5.7	3.4 ± 2.2	4.3 ± 3.6
MOC	1.8 ± 1.4	1.5 ± 1.5	1.1 ± 2.1
Total	1475.4 ± 273.0	1359.6 ± 178.1	1494.9 ± 241.1

Table 4
Mean (±SD; $n = 3$) particle size distribution (μm) of SX original powder (orig. SX), micronised powder (MSX) and SX fractions (produced from the aerosolisation of MSX) deposited on NGI stages ($n = 3$). The data determined by light-scattering corresponding to 10th, median and 90th percentile particle volume-equivalent diameter. '*M*' values represent the stage cut-off mid-range values (μm).

Sample	*M*	$D(v, 0.1)$	$D(v, 0.5)$	$D(v, 0.9)$	D(mode)	Span
S1	10.2	2.9 ± 0.2	9.0 ± 0.6	18.7 ± 1.2	10.8 ± 0.8	1.8 ± 0.0
S2	6.0	2.1 ± 0.1	6.2 ± 0.4	12.0 ± 0.6	7.4 ± 0.5	1.7 ± 0.0
S3	3.6	1.4 ± 0.4	4.4 ± 0.3	9.0 ± 0.7	5.2 ± 0.3	1.7 ± 0.0
S4	2.2	1.0 ± 0.3	3.2 ± 0.2	6.7 ± 0.5	3.5 ± 0.5	1.8 ± 0.1
S5	1.3	0.7 ± 0.1	2.1 ± 0.4	4.7 ± 0.5	2.6 ± 0.3	1.9 ± 0.2
S6	0.7	0.6 ± 0.3	1.3 ± 0.2	3.1 ± 0.2	0.9 ± 0.2	2.0 ± 0.5
MSX	–	0.9 ± 0.1	2.7 ± 0.3	6.9 ± 0.6	2.7 ± 0.2	2.3 ± 0.2

Frequency versus particle size plots (Fig. 3) showed broadly unimodal distributions but with each containing a smaller 'shoulder' at ~0.90 μm. The size of the smaller shoulder appeared to progressively increase as the nominal stage cut-off limit decreased (S1–S4, respectively). Fraction S5, however, displayed a second mode at 0.95 μm while S6 contained a second mode in the size distribution at 2.20 μm. SEM images of fractionated samples show a less disperse size distribution than unfractionated SX samples (Fig. 4).

3.4. The aerodynamic fractionation of FP

Similar to SX, FP fractions produced a sequential decrease in geometric median size when recovered from NGI stages 1–6,

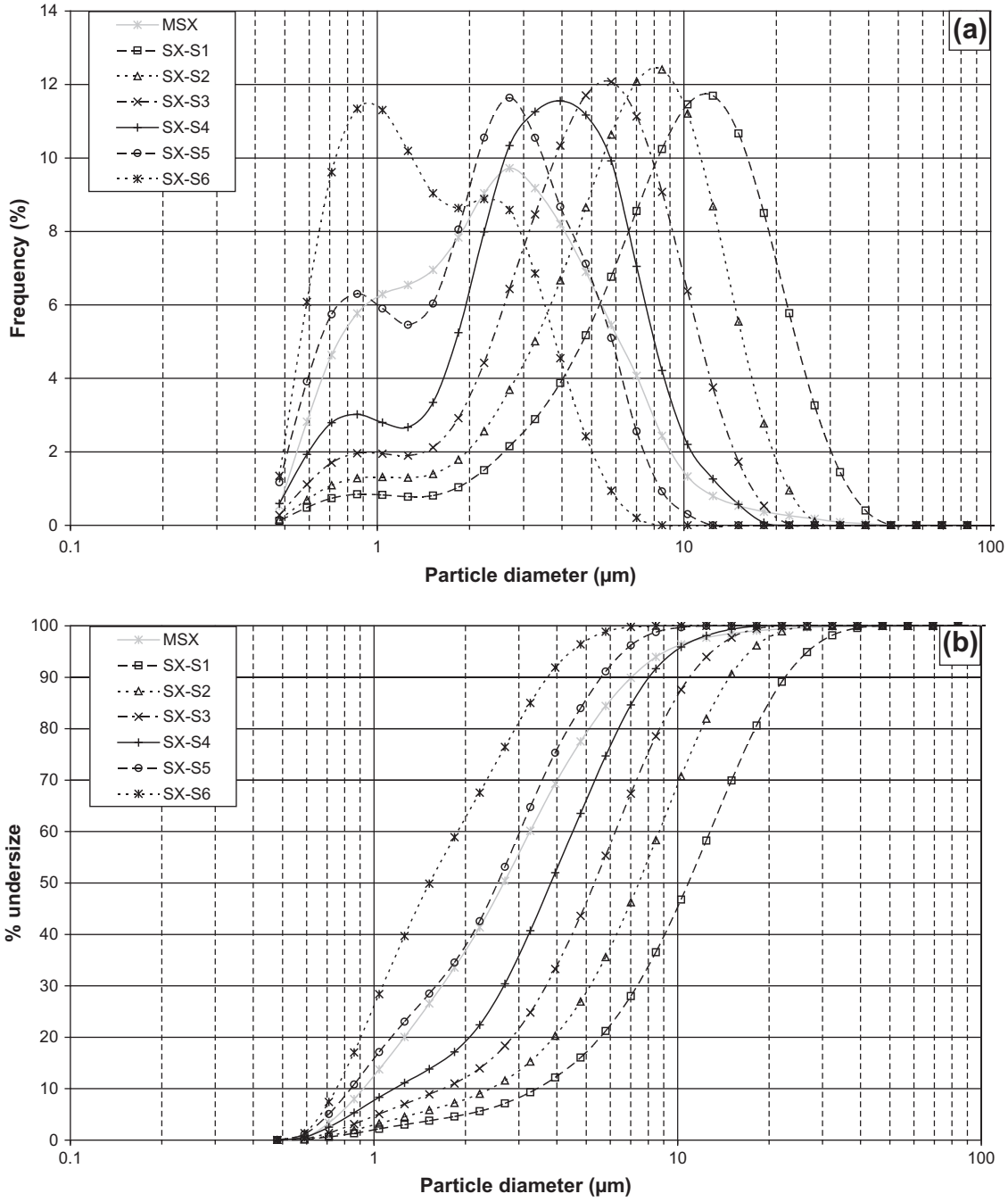

Fig. 3. The geometric volume-equivalent particle diameter of SX fractions recovered from NGI stages 1–6. The mean frequency (a) and % undersize (b) are plotted against particle diameter (μm). $n = 3$.

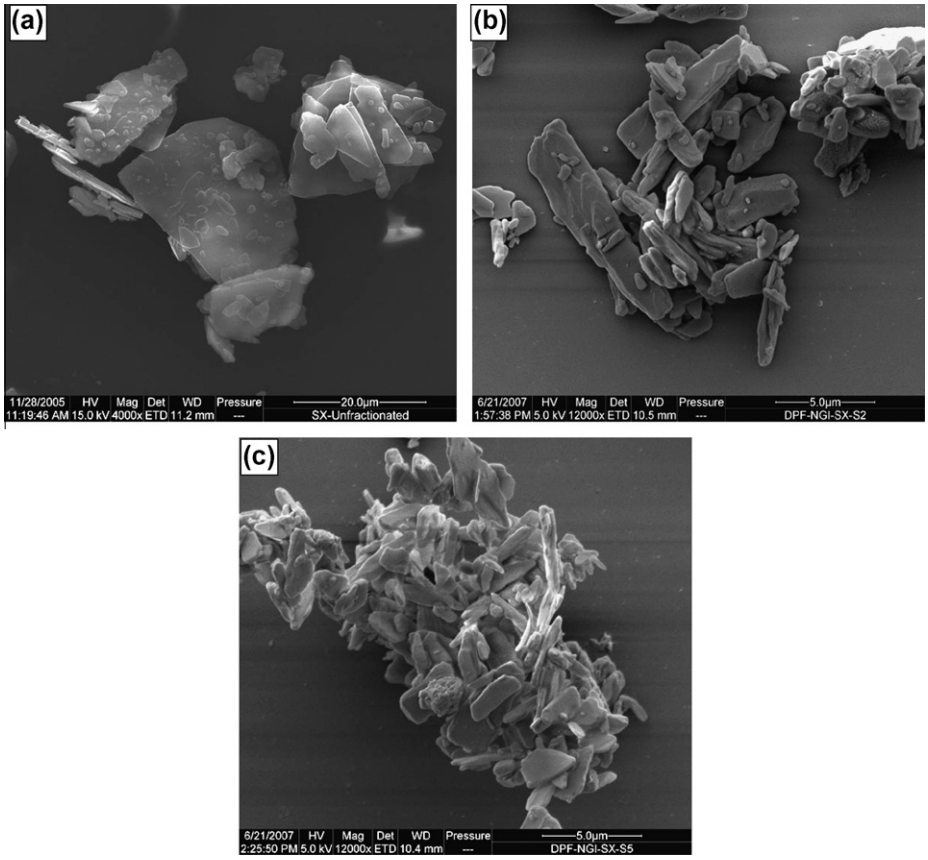

Fig. 4. Representative SEM images of unfractionated SX (a) and fractionated SX samples recovered from NGI stages: S2 (b) and S5 (c). Please note the different scale in image (a).

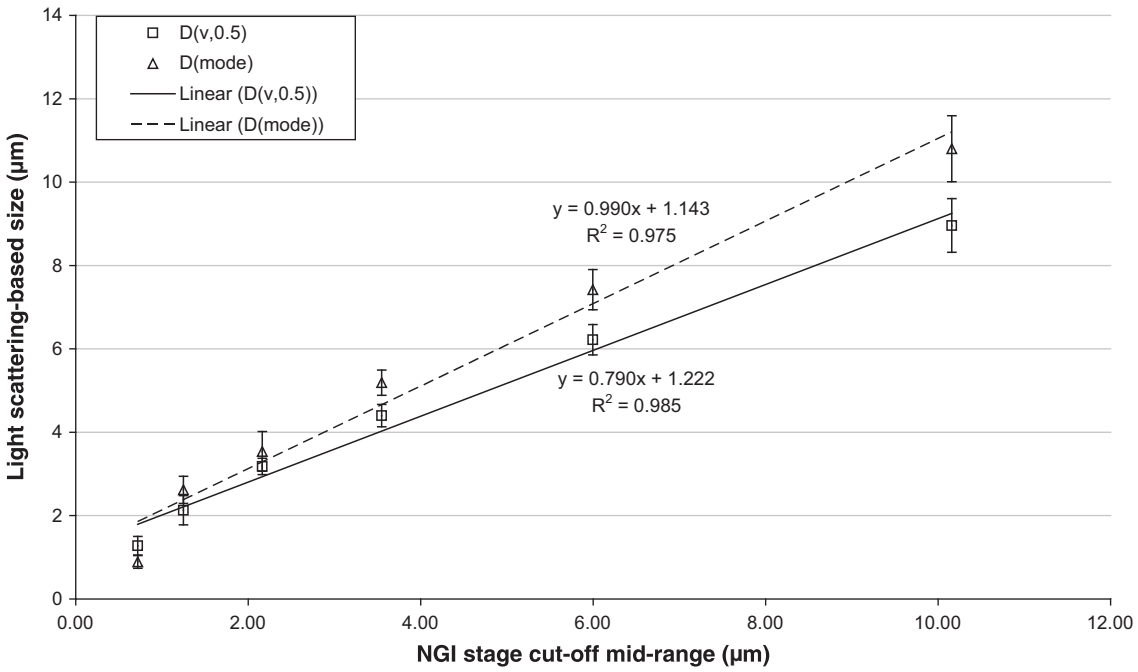

Fig. 5. Linear correlation between the geometric (as determined by light-scattering-based measurements) and aerodynamic particle size (as determined by the NGI) of SX fractions. The graph shows plots of light-scattering-based geometric median [$D(v, 0.5)$] and mode diameters [D(mode)] versus NGI stage cut-off mid-range values ($n = 3$).

respectively (Table 5 and Fig. 6). The original FP had a geometric median size of 4.10 µm and $D(v, 0.1)$ and $D(v, 0.9)$ values of 0.99 µm and 11.21 µm, respectively. All measured diameter values, including $D(v, 0.1)$, $D(v, 0.5)$, $D(v, 0.9)$ and D(mode), showed a

Table 5
Mean (±SD; $n = 3$) particle size distribution (μm) of FP original powder (Orig. FP) and FP fractions deposited on NGI stages (n = 3). The data determined by light-scattering corresponding to 10th, median and 90th percentile particle volume-equivalent diameter. '*M*' values represent the stage cut-off geometric mid-range values (μm).

Sample	*M*	$D(v, 0.1)$	$D(v, 0.5)$	$D(v, 0.9)$	D(mode)	Span
S1	10.2	1.8 ± 0.2	5.7 ± 0.2	11.7 ± 0.6	7.1 ± 0.4	1.7 ± 0.0
S2	6.0	0.9 ± 0.1	3.3 ± 0.1	7.0 ± 0.3	3.7 ± 0.4	1.9 ± 0.0
S3	3.6	0.8 ± 0.1	2.5 ± 0.3	4.7 ± 0.4	2.9 ± 0.3	1.5 ± 0.1
S4	2.2	0.7 ± 0.3	1.7 ± 0.1	3.6 ± 0.4	2.2 ± 0.2	1.7 ± 0.1
S5	1.3	0.7 ± 0.3	1.4 ± 0.1	2.8 ± 0.2	1.4 ± 0.3	1.6 ± 0.1
S6	0.7	0.6 ± 0.3	1.1 ± 0.1	2.5 ± 0.3	0.9 ± 0.2	1.7 ± 0.2
Orig. FP	–	1.0 ± 0.3	4.1 ± 0.3	11.2 ± 0.5	4.3 ± 0.2	2.5 ± 0.1

consistent sequential decrease in size for the powder fractions recovered from stages 1–6, respectively, which correspond to mid-range aerodynamic cut-off values of 10.2–0.7 μm. The geometric median diameters of FP samples recovered from each stage were significantly different (ANOVA, $p < 0.05$). All stages produced samples with significantly smaller span values compared to the original FP powders. EM images of fractionated FP samples show a less disperse particle size distribution compared to unfractionated FP samples (Fig. 7)

A plot of the geometric median and mode diameters of FP fractions against the NGI stage cut-off mid-range values produced highly significant linear relationships ($p < 0.0001$; Fig. 8). The r^2

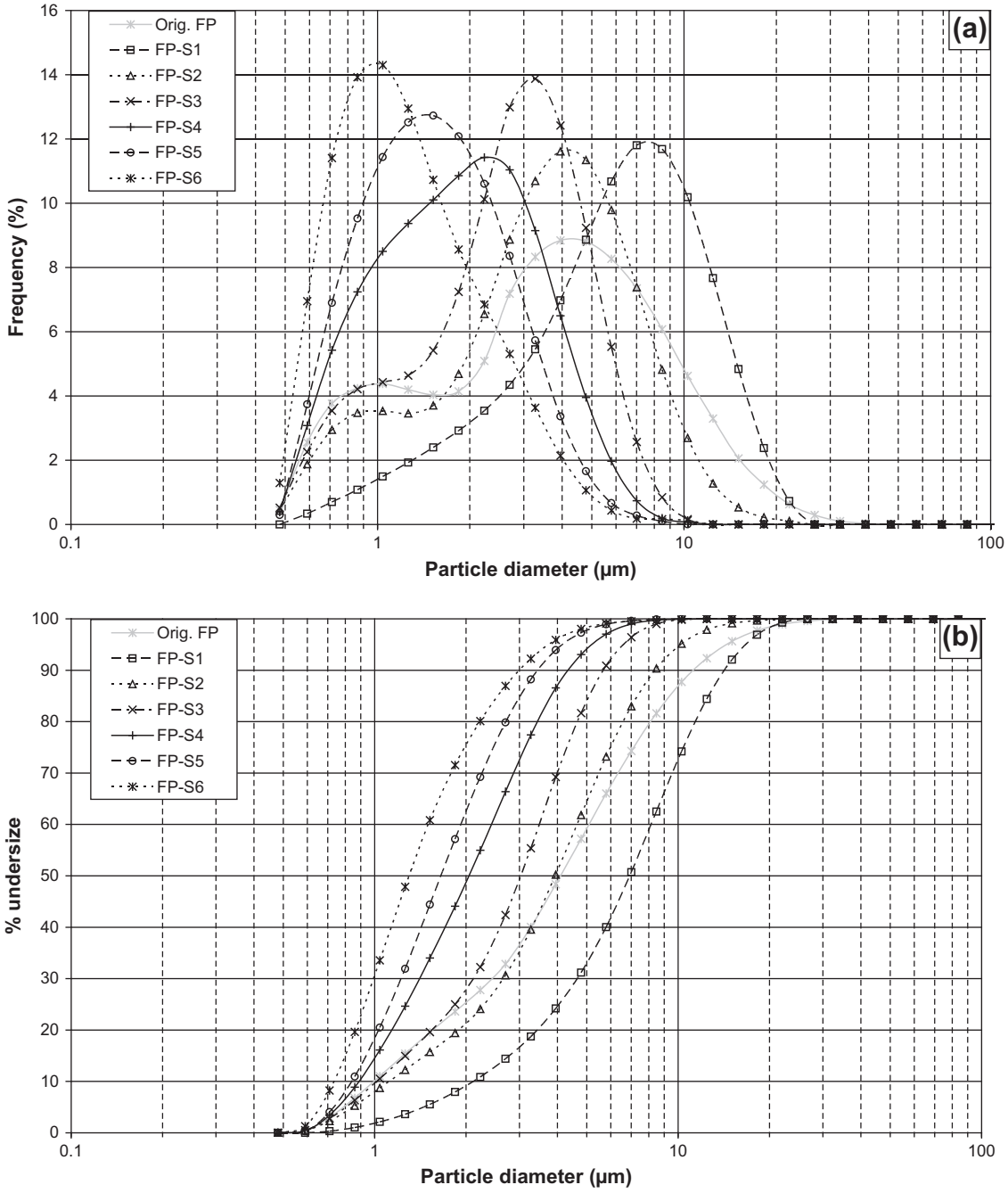

Fig. 6. The geometric volume-equivalent particle diameter of FP fractions recovered from NGI stages 1–6. The mean frequency (a) and % undersize (b) are plotted against particle diameter (μm). $n = 3$.

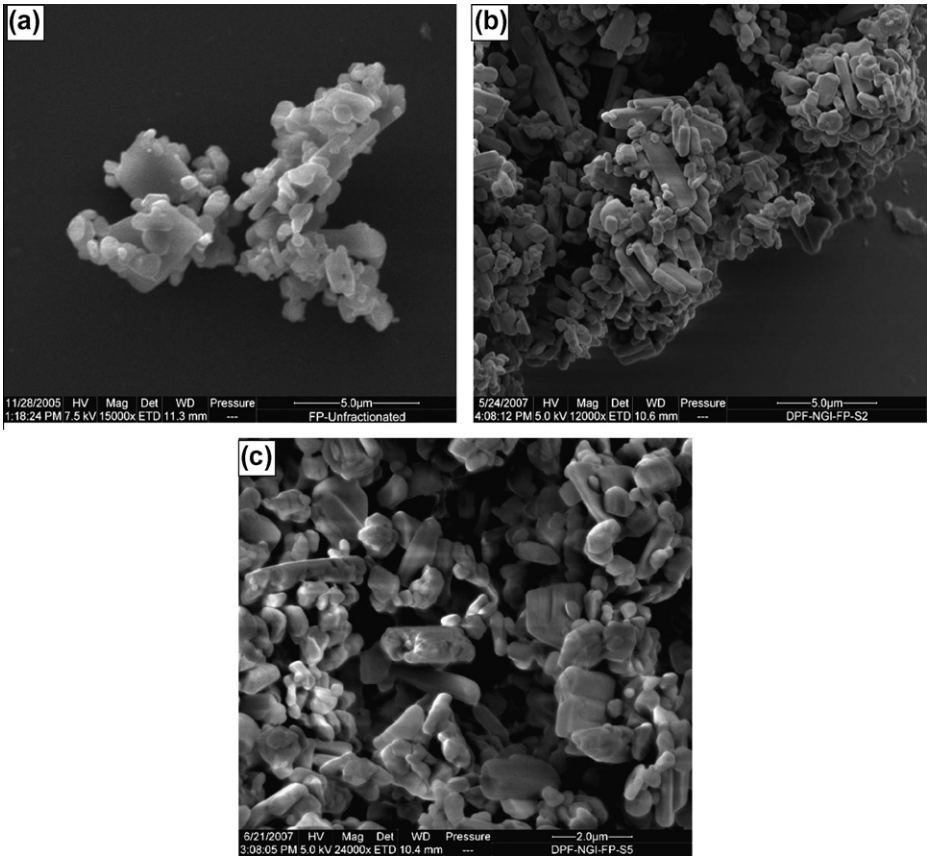

Fig. 7. Representative SEM images of unfractionated FP (a) and fractionated FP samples recovered from NGI stages: S2 (b) and S5 (c). Please note the different scale on the images.

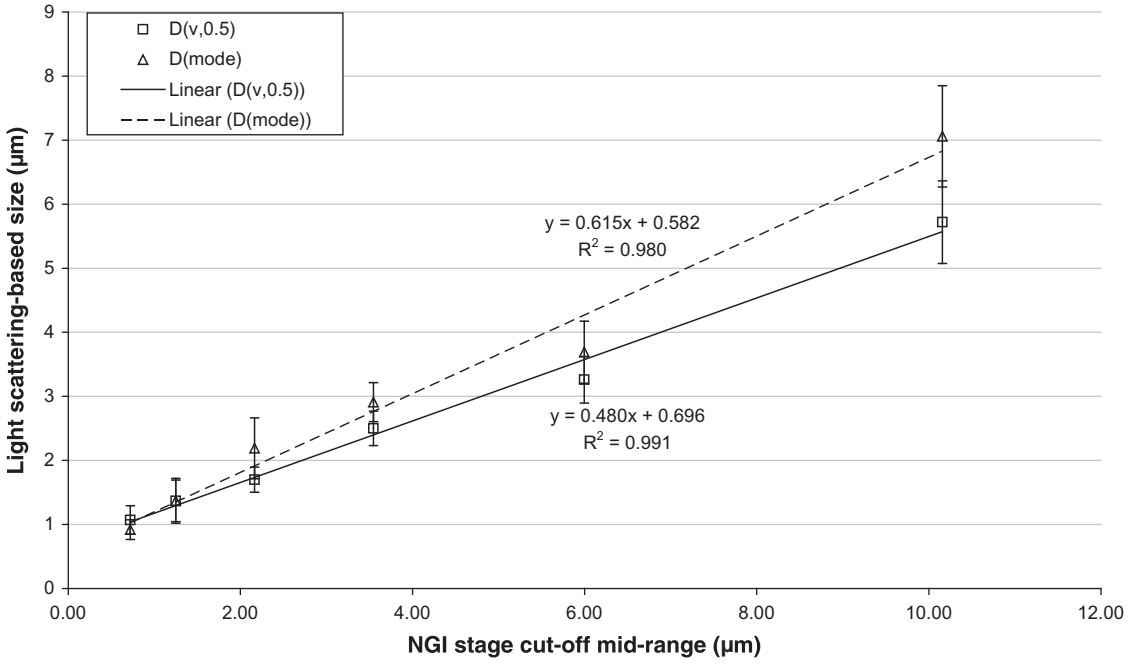

Fig. 8. Linear correlation between the geometric (as determined by light-scattering-based measurements) and aerodynamic particle size (as determined by the NGI) of FP fractions. The graph shows plots of light-scattering-based geometric median [$D(v, 0.5)$] and mode diameters [D(mode)] versus NGI stage cut-off mid-range values ($n = 3$).

values for the median and mode plots were 0.991 and 0.980, respectively. Similar to SX, the mode plot produced a steeper line with a statistically insignificant intercept ($p > 0.05$). Fractions deposited on stages 2 and 3 produced a large mode plus a second

Table 6
Mean (±SD; $n = 3$) particle size distribution (μm) of micronised FL (MFL) and FL fractions deposited on NGI stages ($n = 3$). The data determined by light-scattering corresponding to 10th, median and 90th percentile particle volume-equivalent diameter [mean values ± SD ($n = 3$)]. Light-scattering patterns were analysed according to the Lorenz-Mie theory with the FL 'real' and 'imaginary' refractive indices set at 1.533 and 0.1, respectively, (1.533 + i0.1). '*M*' values represent the stage cut-off mid-range values (μm).

Sample	*M*	$D(v, 0.1)$	$D(v, 0.5)$	$D(v, 0.9)$	D(mode)	Span
S1	10.2	1.2 ± 0.1	6.7 ± 0.3	19.7 ± 0.7	8.1 ± 0.3	2.8 ± 0.0
S2	6.0	1.0 ± 0.2	4.5 ± 0.4	10.2 ± 0.5	6.1 ± 0.4	2.0 ± 0.1
S3	3.6	0.9 ± 0.1	3.2 ± 0.2	6.4 ± 0.2	3.8 ± 0.3	1.7 ± 0.1
S4	2.2	0.9 ± 0.2	2.4 ± 0.3	4.4 ± 0.2	2.6 ± 0.1	1.5 ± 0.2
S5	1.3	0.8 ± 0.2	1.9 ± 0.3	3.7 ± 0.3	2.2 ± 0.2	1.6 ± 0.2
S6	0.7	0.6 ± 0.3	1.1 ± 0.2	2.9 ± 0.1	0.9 ± 0.1	2.0 ± 0.4
MFL	–	0.9 ± 0.2	3.5 ± 0.1	8.9 ± 0.4	3.9 ± 0.1	2.3 ± 0.1

small 'shoulder' at ~0.92 μm while fractions 1, 4, 5 and 6 produced broadly uni-modal size distributions (Fig. 6).

3.5. The aerodynamic fractionation of FL

FL was successfully fractionated producing powder fractions having $D(v, 0.5)$ values between 6.71 and 1.14 μm for stages 1 and 6, respectively (Table 6 and Fig. 9). The FL powder had a pre-fractionation $D(v, 0.5)$ of 3.48 μm. With the exception of FL powder recovered from S1, samples had smaller span values than the pre-fractionation FL powder. A plot of light-scattering obtained median and mode particle diameters versus stage cut-off mid-range values produced significant linear relationships with r^2 values of 0.993 and 0.969, respectively ($p < 0.0001$; Fig. 11). Particle size

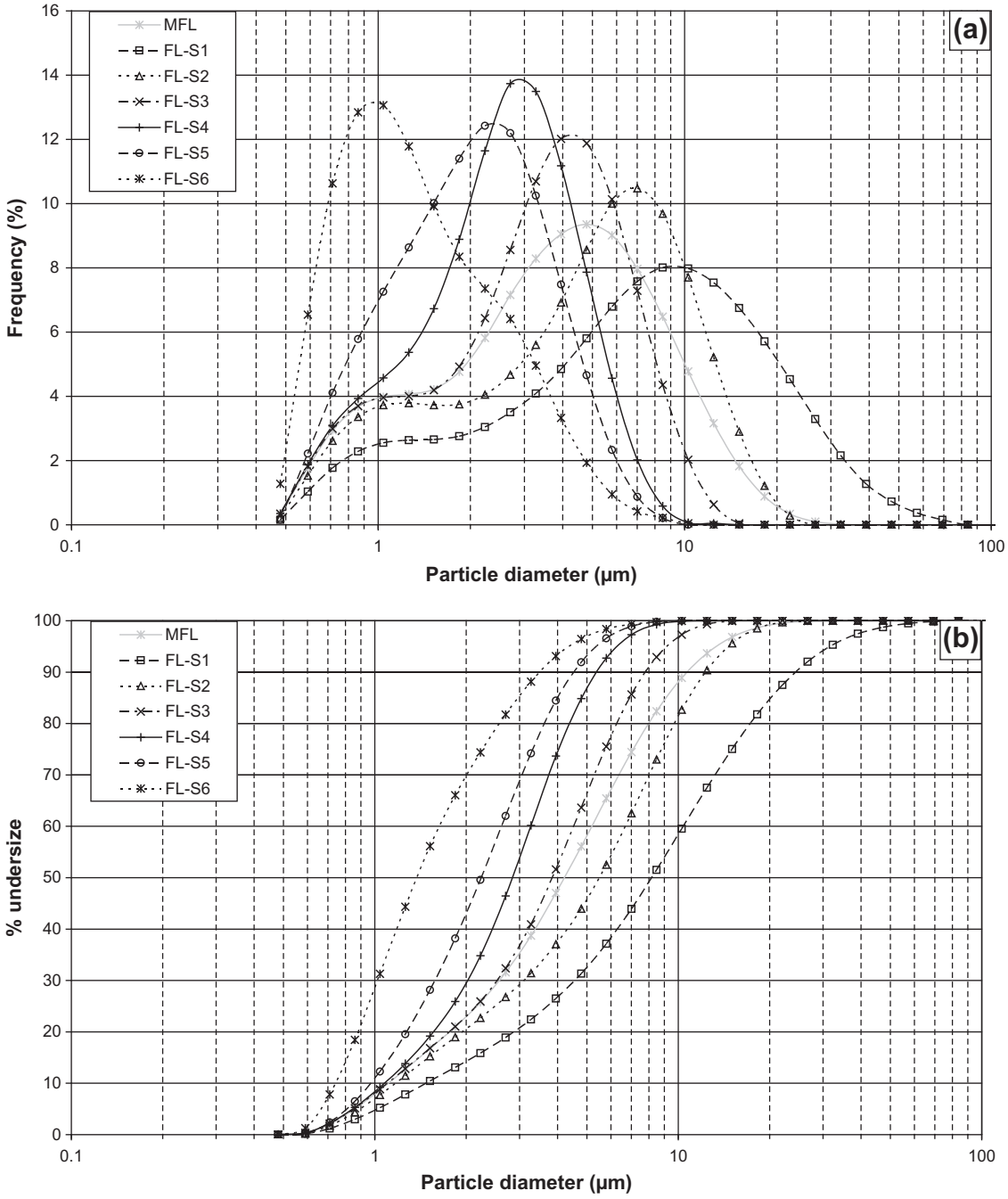

Fig. 9. The geometric volume-equivalent particle diameter of FL fractions recovered from NGI stages 1–6. The frequency (a) and % undersize (b) are plotted against particle size (μm; $n = 3$).

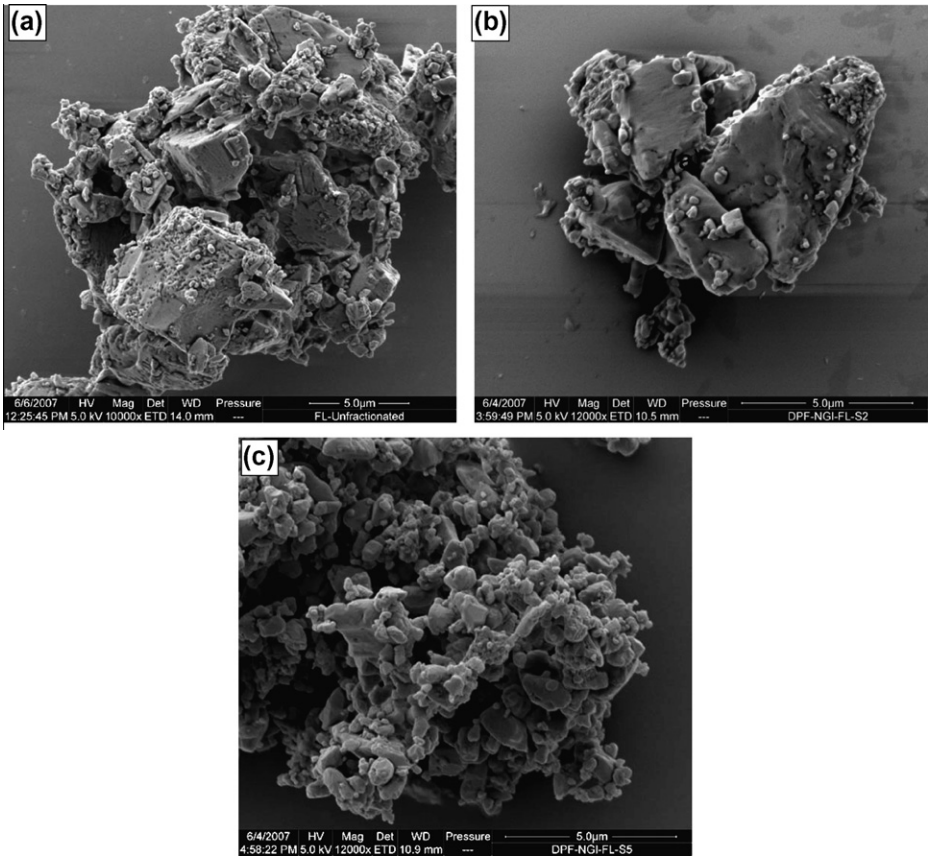

Fig. 10. Representative SEM images of unfractionated FL (a) and fractionated FL samples recovered from NGI stages: S2 (b) and S5 (c). Please note the different scale in image (a).

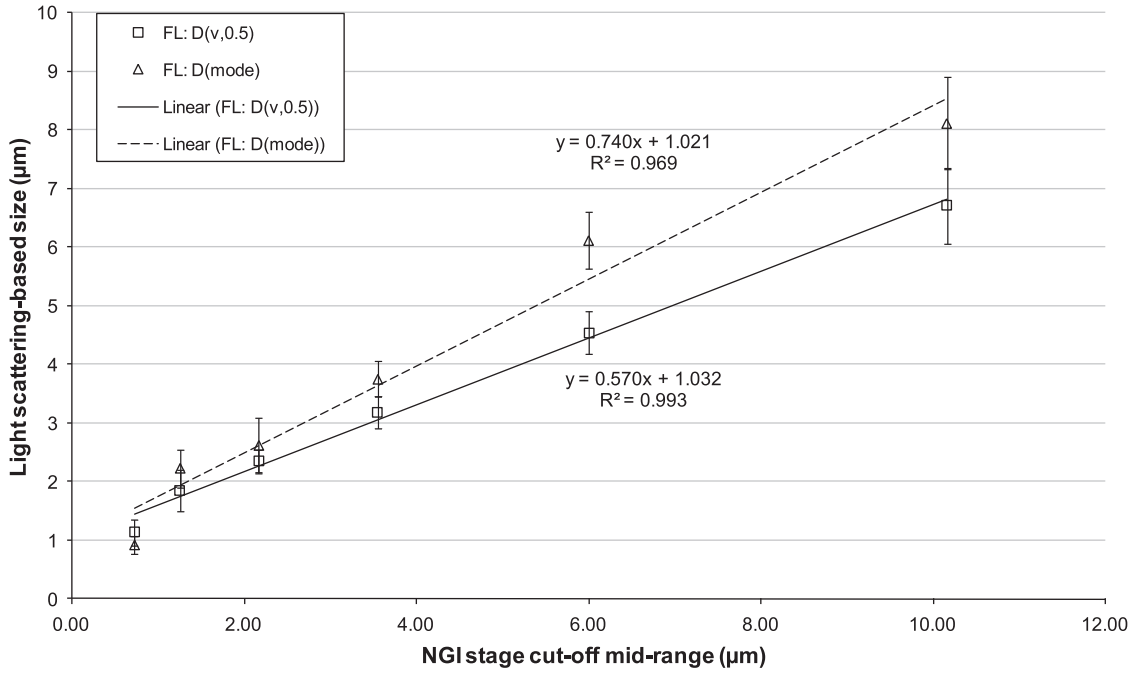

Fig. 11. Linear correlation between the geometric and aerodynamic particle size of FL fractions. The graph shows plots of light-scattering-based geometric median and mode diameters versus NGI stage cut-off mid-range values ($n = 3$).

distribution plots revealed that samples S1–S3 had broad 'tails' extending to the smaller limit of the particle diameter range (Fig. 9). FL SEM images showed a less disperse size distribution in fractionated samples compared to the unfractionated one (Fig. 10).

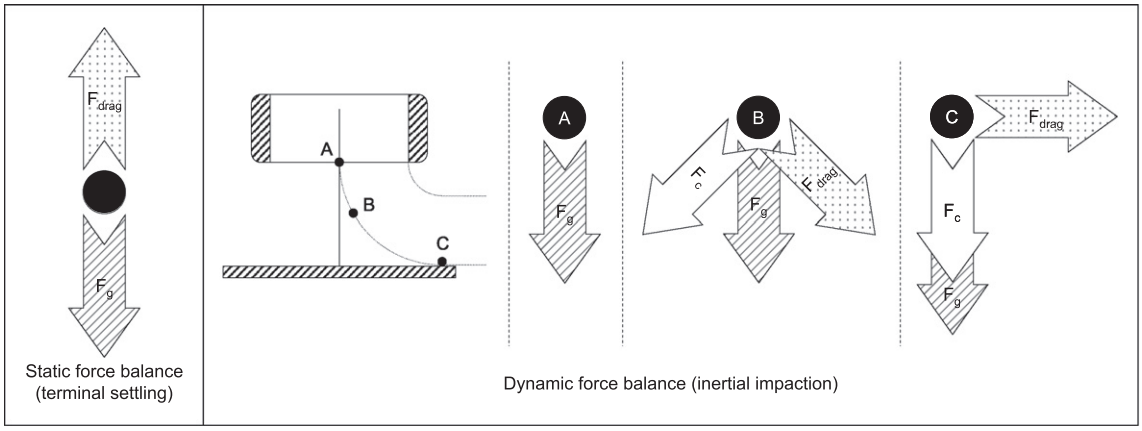

Fig. 12. Schematic presentation of the forces acting on a particle during terminal settling (left) and inertial impaction (right) at three locations (A–C) after leaving the nozzle of an impactor, where F_{drag} is the drag force, F_g is the force of gravity, and F_c is the centrifugal force (Adapted from [38]).

4. Discussion

Successful micronisation by air-jet milling was achieved with SX producing a sample having a $D(v, 0.5)$ value of 2.67 μm. The highly disruptive air-jet milling process has been shown to increase markedly the amorphous content of the powder particularly at the particle surface level [1]. The high energy surface may undergo solid-phase transformations as well as preferential dissolution in condensed water vapour followed by re-recrystallisation into a more stable polymorph – possibly producing solid bridges in the process. FP, on the other hand, had been crystallised by its manufacturers with a median particle size of 4.10 μm.

In the present study, a Malvern QSpec dry powder feeder was employed to aerosolise SX, FP and FL powders. In the Malvern QSpec DPF, powder dispersion is achieved by accelerating particles within a compressed air stream together with particle–particle and particle–wall collisions [22]. The use of the DPF resulted in successful fractionation of SX, FP and FL powders with good recovery. The relative amount of powder depositing on a given NGI stage varied considerably (Table 3). The proportion of powder, by weight, depositing on stage 4 was the largest followed by stage 3. The mid-range NGI cut-off limits of stages 3 and 4 at a flow rate of 60 L min^{-1} are 3.6 and 2.2 μm, respectively, with particles having a nominal aerodynamic diameter between 1.66 and 4.46 μm expected to deposit on one of the two stages. The greater deposition on stages 4 and 3 observed may be expected given that SX and FL powders had already been micronised to median sizes within the 1.66–4.46 μm range (Tables 4 and 6, respectively) and that the solvent-crystallised FP powder used in the fractionation process had a measured median size of 4.10 μm (Table 5). Additionally, with the FP powder having the largest pre-fractionation $D(v, 0.5)$ and $D(v, 0.9)$ values, a greater percentage of pre-separator deposition was expected and was observed – as FP had the lowest total recovery from NGI stages (68%, Table 3) compared to SX and FL.

The median diameter $D(v, 0.1)$ and $D(v, 0.9)$ values for fractions recovered from stages 1–6 of the NGI increased sequentially confirming that successful fractionation had taken place for all of SX, FP and FL. Cumulative frequency versus particle diameter plots for fractions recovered from stages 1–6 for all three powders showed lines that were generally parallel and equally spaced along the *x*-axis (Figs. 3b, 6b and 9b). In each case, fractions had smaller span values compared to the pre-fractionation powder as expected, except for the FL-S1 fraction (Table 6). This may have resulted from some particles depositing in the lower compartment of the pre-separator becoming detached and falling into the stage 1 cup during one of the disassembly routines at some stage in the FL fractionation process.

A degree of overlap between the frequency versus particle diameter plots of fractions recovered from NGI stages was observed for all three powders (Figs. 3a, 6a and 9a). An ideal impactor should show no overlap between the efficiency curves of its stages. However, a small degree of overlap has been demonstrated between the efficiency curves of the stages of available impactors including the NGI [23,24]. Nevertheless, the degree of overlap observed in the frequency versus geometric particle size plots was larger than that observed in the calibration of the NGI [25]. Separation of particles in the NGI is based on the aerodynamic size of the particle. The aerodynamic size is a function of the particle's density and shape as well as its geometric size. Consequently, two different particles may have different geometric diameters despite sharing a similar aerodynamic particle size and vice versa. Therefore, the observed overlap between the geometric size of particles recovered from different NGI stages does not necessarily reflect a similar degree of overlap in their aerodynamic size.

Some overlap in the frequency versus geometric particle size plots could also be due to the assumption that a portion of particles deposit on NGI stages as agglomerates. Despite the high dispersion efficiency of the DPF, some strongly adhered particles may still be entrained as agglomerates. Once dispersed in a liquid medium with the aid of ultrasonication, these agglomerates are likely to break-up producing multiple small particles which skew the laser diffraction particle size distribution towards smaller sizes. Such strongly held agglomerates are unlikely to be dispersed upon aerosolisation using a typical DPI device.

Cascade impactors, including the NGI, have been shown to suffer from a small degree of 'particle bounce', where a particle may deposit on a given NGI stage but becomes re-entrained in the air stream and consequently deposits on another NGI stage with a smaller nominal cut-off diameter [26,27]. Particle bounce can be minimised by coating the impaction plates with a viscous liquid [28]. However, the use of stage coating is inappropriate in this study, as deposits will not be recoverable in a dry powder form. The necessary omission of stage coating may have resulted in an increased degree of particle bounce and a consequent increased overlap between the frequency curves of samples recovered from different NGI stages. Particle bounce is expected to result in an underestimation of aerodynamic size particularly in samples deposited on the earlier NGI stages due to higher Reynolds numbers in stages having larger cut-off diameters [24]. However, the geometric particle size measurements of recovered FP and FL fractions were generally smaller than their nominal aerodynamic sizes for powders collected in stages 1–3 (Tables 4 and 6) which may suggest that the effect of particle bounce on the particle size distribution of fractionated powders was not important. In SX, the geometric sizes were generally larger than

the aerodynamic ones, except for SX-S1 (Table 4). However, considering that the experimental parameters were similar for all three compounds and that a highly linear correlation between aerodynamic and geometric SX measurements was obtained (Fig. 5), the effect of particle bounce on SX may also have been unimportant.

Considering the frequency versus particle diameter plots for SX, FP and FL fractions (Figs. 3a, 6a and 9a, respectively), peak shapes for fractions 1–4 were generally symmetrical with some tailing towards smaller particle diameters. Such tailing and/or secondary modes may have resulted from agglomerated fine particles depositing on stages with larger nominal cut-off limits. The small particle sizes of the pre-fractionation powders were expected to render them highly cohesive. Agglomerates that might have been aerosolised without effective de-agglomeration may be expected to have an aerodynamic size akin to that of a single particle with a similar size, shape and density to those exhibited by the agglomerate rather than an aerodynamic size corresponding to the primary particles forming the agglomerate. Such agglomerated particles, therefore, may deposit on stages with larger nominal cut-off diameters than expected. However, when powders are recovered and prepared for measurement by the Malvern Mastersizer, samples are suspended in a liquid and subjected to ultrasonic waves resulting in the break-up of agglomerates into their primary particles. Such particles may appear as a 'tail' in the frequency versus particle diameter plots. It is also possible that these tails may have resulted from slight errors in the imaginary component of the refractive index used in calculations performed by the Mastersizer [29,30].

Correlations between droplet/particle size measurements obtained via light-scattering and inertial impaction have been reported using nebulised solutions [31,32], pMDI generated sprays [33,34] and DPI aerosols [17,35–37]. Researchers have generally quantified the deposits recovered from various impactor stages to obtain overall MMAD and GSD values which were then compared to equivalent light-scattering-derived measurements obtained from analyses performed on the powder. Effectively, comparisons are based on a single MMAD of a given aerosolised sample. However, there are no published reports comparing a series of samples with small aerodynamic differences to geometric measurements obtained for narrow-distribution samples within the size range of respirable particles. In this study, the generation of several samples containing particles grouped on basis of their aerodynamic size provided a unique opportunity for producing correlations between the aerodynamic and geometric size of respirable particles on basis of multiple samples.

The drag force acting on a particle suspended in air under laminar flow conditions can be expressed in terms of Stokes' law:

$$F_{\text{drag}} = \frac{3\pi\eta d_p \chi V}{C_c} \tag{3}$$

where F_{drag} is the drag force, η is the viscosity of air, d_p is the particle diameter, χ is the dynamic shape factor of the particle, defined as the actual resistance force acting on the particle relative to the resistance force acting on a spherical particle having the same volume and velocity, V is the air velocity and C_c is the Cunningham slip correction factor [5].

When the particle reaches its terminal settling velocity, it is acted upon by two forces that are equal in magnitude and opposite in direction. They are the drag force (F_{drag}) and the force of gravity (F_g). Therefore:

$$\frac{\pi}{6} d_p^3 \rho_p g = F_g = F_{\text{drag}} = \frac{3\pi\eta d_p \chi V_{ts}}{C_c} \tag{4}$$

where d_p is the particle diameter, ρ_p is the particle density, g is the gravitational acceleration, η is the viscosity of air, χ is the dynamic shape factor of the particle, V_{ts} is the terminal settling velocity of the particle and C_c is the Cunningham slip correction factor. Consequently:

$$V_{ts} = \frac{d_p^2 \rho_p g C_c}{18\eta\chi} \tag{5}$$

Considering that the aerodynamic particle size (d_{ae}) is defined as the diameter of a unit density sphere having the same terminal settling velocity as the particle, d_{ae} can be expressed in terms of d_p provided that laminar air flow conditions are maintained and that the size of the particle is much larger than the mean free path of a molecule in air ensuring that the medium is continuous (as experienced by the particle), thus avoiding the need for slip correction (C_c):

$$d_{ae} = d_p \sqrt{\left(\frac{\rho_p}{\rho_0 \chi}\right)} \tag{6}$$

where ρ_0 is unit density (1 g cm^{-3}). Based on Eq. (6), the gradient of a line fitted through data points representing the geometric particle size as measured by the Mastersizer versus NGI stage cut-off mid-range values is given by:

$$\text{Gradient} = \left(\frac{\rho_p}{\rho_0 \chi}\right)^{-0.5} \tag{7}$$

It has been suggested that the crystal density (ρ_p) of most inhaled drugs is between 1.2 and 1.5 g cm^{-3} and that dynamic shape factor (χ) values are also $\geqslant 1$ for single particles, the two values should compensate for each other producing similar values for d_{ae} and d_p [38]. The actual density values (±SD) of SX, FP and FL crystals are 1.24 (±0.01), 1.40 (±0.01) and 1.55 (±0.02) g cm^{-3}, respectively. The SX $D(v, 0.5)$ and D(mode) versus aerodynamic mid-range cut-off limits best-fit lines (Fig. 5) have gradients of 0.790 and 0.990 resulting in calculated χ values of 0.77 and 1.21, respectively. For FP, the $D(v, 0.5)$ and D(mode) best-fit lines' gradient values were 0.480 and 0.615 resulting in calculated χ values of 0.32 and 0.53, respectively (Fig. 8). The calculated χ values for FL were 0.50 and 0.85 resulting from the best-fit lines' gradient values for $D(v, 0.5)$ and D(mode) of 0.57 and 0.74, respectively (Fig. 11). Single spherical particles have a χ value of 1 while non-spherical ones have values >1. The χ value for SX D(mode) is well within the expected range, however, FP and FL values are low. It is possible for the (ρ_p/χ) value to be <1 when small clusters are present particularly as chains of strongly attached particles [38]. However, the correlation between d_{ae} and d_p expressed in Eq. (6) is only valid on basis of several assumptions including that the particle size is much larger than the mean free path of a molecule in air (approximately 66.5 nm) such that the gas medium experienced by the particle can be considered continuous. This assumption is not fully satisfied particularly for samples depositing on stage 6 where a large proportion of particles had a diameter <1 μm. The condition may have not been satisfied either for a significant proportion of particles depositing on other stages (Figs. 3, 6 and 9). Another assumption made in Eq. (6) for d_{ae} to correlate with d_p is that laminar airflow conditions are maintained. It has been suggested that cascade impactors, including the NGI, should be operated with Reynolds numbers between 500 and 3000 to ensure such laminar flow conditions [23,38]. The Re numbers for the NGI stages 1 and 2 at 60 L min^{-1} are 5876 and 2870, respectively [23]. Local violations to laminar conditions may still exist in areas of sharp change in the direction of air flow even below the upper Re limit of 3000 [38,39].

Particle shape has been shown to influence particle size measurements performed by different techniques to a different degree which can lead to poor inter-method correlations [40–42]. Light-scattering-based instruments may under- or over-estimate the size of non-spherical particles depending on the measurement conditions [43]. Measurement of the aerodynamic particle size by different instruments can also vary as a result of particle shape [16]. During the terminal settling of a particle in a stationary air medium, the drag force acting on the particle is constant ($F_{\text{drag}} = F_g$).

In contrast, during inertial impaction and in addition to drag and gravity forces, a particle is acted upon by a centrifugal force resulting from the particle's change of direction. The centrifugal and drag forces change depending on the particle's position between the impactor nozzle and the impaction plate (Fig. 12). In this dynamic system of forces, irregularly shaped particles may exhibit a different behaviour from that displayed during terminal stationary settling conditions. The particle may start to rotate, constantly changing its χ value, which may result in a different average χ to that exhibited during stationary settling conditions [38]. The numerical difference observed between d_{ae} and $D(v, 0.5)$ and D(mode) may, therefore, be explained considering the possible violation of the assumptions made in the derivation of Eq. (6). However, the small standard deviation values shown in Tables 4–6 and the high statistical significance obtained for the $D(v, 0.5)$ and D(mode) best-fit lines for all of SX, FP and FL ($p < 0.0001$) may validate the linear correlations between the aerodynamic and geometric particle size of each of SX, FP and FL samples produced by aerodynamic fractionation in the present study.

Milling (e.g. jet-milling) is the most widely used method for the production of micronised particles for use in DPIs, pMDIs and nebulised suspension formulations [44,45]. Milling techniques, however, suffer from important disadvantages including local heat generation which may render milling techniques less suitable for heat-sensitive biopharmaceuticals such as peptides [46,47]. In contrast, controlled crystallisation techniques [9,11,14,48] have been shown to produce highly crystalline respirable particles. However, crystallisation techniques suffer from disadvantages, including manufacturing complexity, limited particle size control and being material-specific necessitating the redevelopment or adaptation of the method depending on the material being generated in the micronised state. Spray-drying techniques are well established but typically produce amorphous particles which can suffer from solid-state instability problems [49,50]. Furthermore, reported techniques for the production of micron-sized particles, to-date, do not offer any degree of precise control over the aerodynamic size of particles produced. Consequently, the aerodynamic fractionation method presented in this study offers a major advantage by enabling precise control of the aerodynamic size of particles in a given sample. The upper and lower aerodynamic size limits of fractions can be easily controlled by the prior choice of the NGI flow rate and impaction stage for particle collection.

The present method is not material-specific and should result in no compromise in terms of the chemical and physical stability of the powder. However, the fractionation technique is not a micronisation method in its own right and cannot be used without having particles of the desired size present in the pre-fractionation powder mix, and this consequently results in an added step in the production of the micron-sized particles. In the present study, SX and FL were micronised prior to fractionation while FP was simply solvent-crystallised following synthesis. However, the production of micro-particles in a 'crude' mix is a readily achievable process since almost all respirable powders undergo a crystallisation process at some point following their chemical synthesis in solution. A compound can be easily precipitated from solution ensuring the production of 'some' micron-sized particles in the process, regardless of the presence of larger particles, such as by the addition of a solution containing the material into an anti-solvent with efficient mixing. Such a 'crude' mix of particle sizes produced by crystallisation followed by fractionation should result in narrow size distribution powders containing largely crystalline particles in the desired aerodynamic size range. The whole process of production and fractionation may well be less costly and time consuming than micronisation or spray-drying, let alone developing a compound-specific micronisation-by-crystallisation technique. However, considering the impactors available at present, the fractionation method is not likely to be an efficient production-scale process for obtaining micron-sized particles. Nonetheless, this study demonstrates the concept of aerodynamic fractionation as a preparative technique. The main principles discussed herein can be adapted, such as through the use of a virtual impactor or a train of cyclones, to allow for a high throughput scalable process.

Nevertheless, the present fractionation method should offer a valuable research tool that can produce unique narrow-distribution samples of controlled aerodynamic sizes allowing for focused investigations into the effect of small changes in particle size on the *in vitro* and *in vivo* performance of aerosols. Powders produced by the fractionation method can be particularly useful for investigating the fundamental drug–drug and/or drug–excipient interactions in multi-component formulations (e.g. combination products) through the production of samples having 'equivalent' aerodynamic size distributions. Such a technique would be applicable to the generation of various drugs and excipients in a suitable size for inhalation. Powders produced by fractionation may also be employed for investigating the role of physico-chemical properties other than particle size distribution in determining aerodynamic deposition. The production of aerodynamically equivalent fractions is feasible enabling deposition discrepancies resulting from differences in the particle size distribution of the primary powders to be minimised. Additionally, comparisons between aerodynamically equivalent primary powders produced by the various micronisation techniques, such as controlled crystallisation, milling and spray-drying, can be made.

5. Conclusion

Despite the availability of various methods for the production of micron-sized particles, such as, milling, controlled crystallisation and spray-drying, precise control of the aerodynamic size distribution of powders produced by available methods remains a challenge. In the present study, SX and FL powders were jet-milled. Crystallised FP and jet-milled SX and FL samples were then aerodynamically fractionated using a system comprising the Malvern QSpec dry powder feeder and the NGI. Fractions were then recovered from NGI stages and had their particle size distributions assessed by light-scattering.

The fractionation process was successful for all powders producing significant linear correlations between the pre-set aerodynamic cut-off limits and geometric size measurements. For each of SX, FP and FL, sufficient powder quantities were recovered from NGI stages 1–6 producing six fractions with sequential aerodynamic and geometric particle size distributions. Light-scattering particle size measurements confirmed that fractions had narrow geometric particle size distributions with mean span values for SX, FP and FL of 1.80, 1.68 and 1.93, respectively, compared to the original powders which had span values of 2.25, 2.49 and 2.27, respectively.

The fractionation method described in the present study was efficient and reproducible for all powders studied (SX, FP and FL). The method can be equally applied to various drugs and excipients regardless of their previous method of production, including crystallisation, spray-drying and milling. The present method may, therefore, be used to compare and contrast samples produced by different techniques.

The fractionation method may have advantages over available techniques particularly in terms of producing aerodynamically equivalent samples. Such samples may be advantageous including when used to investigate drug–drug and drug–excipient interactions in combination formulations.

Acknowledgement

The authors gratefully acknowledge TEVA Pharmaceuticals for funding this work.

References

[1] G. Buckton, A. Choularton, A.E. Beezer, S.M. Chatham, The effect of the comminution technique on the surface energy of a powder, Int. J. Pharm. 47 (1988) 121–128.

[2] H. Steckel, N. Rasenack, B.W. Muller, In-situ-micronization of disodium cromoglycate for pulmonary delivery, Eur. J. Pharm. Biopharm. 55 (2003) 173–180.

[3] L. Mackin, R. Zanon, J.M. Park, K. Foster, H. Opalenik, M. Demonte, Quantification of low levels (<10%) of amorphous content in micronised active batches using dynamic vapour sorption and isothermal microcalorimetry, Int. J. Pharm. 231 (2002) 227–236.

[4] H.K. Chan, N.Y.K. Chew, Novel alternative methods for the delivery of drugs for the treatment of asthma, Adv. Drug Del. Rev. 55 (2003) 793–805.

[5] X.M. Zeng, G.P. Martin, C. Marriott, Particulate Interactions in Dry Powder Formulations for Inhalation, first ed., Taylor & Francis, London, UK, 2001.

[6] M.T. Vidgren, P.A. Vidgren, T.P. Paronen, Comparison of physical and inhalation properties of spray-dried and mechanically micronized disodium cromoglycate, Int. J. Pharm. 35 (1987) 139–144.

[7] P. Harjunen, V.P. Lehto, K. Martimo, E. Suihko, T. Lankinen, P. Paronen, K. Jarvinen, Lactose modifications enhance its drug performance in the novel multiple dose Taifun DPI, Eur. J. Pharm. Sci. 16 (2002) 313–321.

[8] H. Larhrib, G.P. Martin, C. Marriott, D. Prime, The influence of carrier and drug morphology on drug delivery from dry powder formulations, Int. J. Pharm. 257 (2003) 283–296.

[9] K. Ikegami, Y. Kawashima, H. Takeuchi, H. Yamamoto, N. Isshiki, D.I. Momose, K. Ouchi, Primary crystal growth during spherical agglomeration in liquid: designing an ideal dry powder inhalation system, Powder Technol. 126 (2002) 266–274.

[10] N. Rasenack, H. Steckel, B.W. Muller, Micronization of anti-inflammatory drugs for pulmonary delivery by a controlled crystallization process, J. Pharm. Sci. 92 (2003) 35–44.

[11] J.S. Kaerger, R. Price, Processing of spherical crystalline particles via a novel solution atomization and crystallization by sonication (SAXS) technique, Pharm. Res. 21 (2004) 372–381.

[12] J.M. Lobo, H. Schiavone, S. Palakodaty, P. York, A. Clark, S.T. Tzannis, SCF-engineered powders for delivery of budesonide from passive DPI devices, J. Pharm. Sci. 94 (2005) 2276–2288.

[13] H. Schiavone, S. Palakodaty, A. Clark, P. York, S.T. Tzannis, Evaluation of SCF-engineered particle-based lactose blends in passive dry powder inhalers, Int. J. Pharm. 281 (2004) 55–66.

[14] M. Rehman, B.Y. Shekunov, P. York, D. Lechuga-Ballesteros, D.P. Miller, T. Tan, P. Colthorpe, Optimisation of powders for pulmonary delivery using supercritical fluid technology, Eur. J. Pharm. Sci. 22 (2004) 1–17.

[15] B.Y. Shekunov, J.C. Feeley, A.H.L. Chow, H.H.Y. Tong, P. York, Aerosolisation behaviour of micronised and supercritically-processed powders, J. Aerosol Sci. 34 (2003) 553–568.

[16] T.M. Crowder, J.A. Rosati, J.D. Schroeter, A.J. Hickey, T.B. Martonen, Fundamental effects of particle morphology on lung delivery: predictions of Stokes' law and the particular relevance to dry powder inhaler formulation and development, Pharm. Res. 19 (2002) 239–245.

[17] C. Bosquillon, C. Lombry, V. Preat, R. Vanbever, Comparison of particle sizing techniques in the case of inhalation dry powders, J. Pharm. Sci. 90 (2001) 2032–2041.

[18] D.L. French, D.A. Edwards, R.W. Niven, The influence of formulation on emission, deaggregation and deposition of dry powders for inhalation, J. Aerosol Sci. 27 (1996) 769–783.

[19] W.I. Li, M. Perzl, J. Heyder, R. Langer, J.D. Brain, K.H. Englmeier, R.W. Niven, D.A. Edwards, Aerodynamics and aerosol particle deaggregation phenomena in model oral-pharyngeal cavities, J. Aerosol Sci. 27 (1996) 1269–1286.

[20] D. Prime, The SX and FP refractive index values, in, GSK, personal communication 2008.

[21] H. Adi, I. Larson, P. Stewart, Laser diffraction particle sizing of cohesive lactose powders, Powder Technol. 179 (2007) 90–94.

[22] Malvern Instruments Ltd., Data Sheet: QSpec dry powder feeder, 2008. <http://www.malvern.co.uk/LabEng/products/Mastersizer/MSS/qspec_dpf.htm> (accessed 25.06.08).

[23] V.A. Marple, D.L. Roberts, F.J. Romay, N.C. Miller, K.G. Truman, M. Van Oort, B. Olsson, M.J. Holroyd, J.P. Mitchell, D. Hochrainer, Next generation pharmaceutical impactor (a new impactor for pharmaceutical inhaler testing). Part I: Design, J. Aerosol Med.: Depos. Clearance Effects Lung 16 (2003) 283–299.

[24] J.P. Mitchell, M.W. Nagel, Cascade impactors for the size characterization of aerosols from medical inhalers: their uses and limitations, J. Aerosol Med.: Depos. Clearance Effects Lung 16 (2003) 341–377.

[25] V.A. Marple, B.A. Olson, K. Santhanakrishnan, J.P. Mitchell, S.C. Murray, B.L. Hudson-Curtis, Next generation pharmaceutical impactor (a new impactor for pharmaceutical inhaler testing). Part II: Archival calibration, J. Aerosol Med.: Depos. Clearance Effects Lung 16 (2003) 301–324.

[26] J.P. Mitchell, M.W. Nagel, K.J. Wiersema, C.C. Doyle, Aerodynamic particle size analysis of aerosols from pressurized metered-dose inhalers: comparison of Andersen 8-stage cascade impactor, next generation pharmaceutical impactor, and model 3321 aerodynamic particle sizer aerosol spectrometer, AAPS Pharm. Sci. Technol. 4 (4) (2003) Article 54.

[27] A. Kamiya, M. Sakagami, M. Hindle, P.R. Byron, Aerodynamic sizing of metered dose inhalers: an evaluation of the Andersen and next generation pharmaceutical impactors and their USP methods, J. Pharm. Sci. 93 (2004) 1828–1837.

[28] Ph. Eur., Consistency of Formulated Preparations: Fine Particle Dose and Particle Size Distribution, in: European Pharmacopoeia, European Directorate for the Quality of Medicines and Healthcare, 2004.

[29] International Organization for Standardization, Particle Size Analysis-Laser Diffraction Methods – Part 1: General Principles, 1999, ISO 13320-13321: 11999(E).

[30] A. Beekman, D. Shan, A. Ali, W. Dai, S. Ward-Smith, M. Goldenberg, Micrometer-scale particle sizing by laser diffraction: critical impact of the imaginary component of refractive index, Pharm. Res. 22 (2005) 518–522.

[31] W.T.J. Kwong, S.L. Ho, A.L. Coates, Comparison of nebulized particle size distribution with Malvern laser diffraction analyzer versus Andersen cascade impactor and low-flow Marple personal cascade impactor, J. Aerosol Med.: Depos. Clearance Effects Lung 13 (2000) 303–314.

[32] L. Vecellio None, D. Grimbert, M.H. Becquemin, E. Boissinot, A. Le Pape, E. Lemarie, P. Diot, Validation of laser diffraction method as a substitute for cascade impaction in the European project for a nebulizer standard, J. Aerosol Med.: Depos. Clearance Effects Lung 14 (2001) 107–114.

[33] A. Haynes, M.S. Shaik, H. Krarup, M. Singh, Evaluation of the Malvern Spraytec with inhalation cell for the measurement of particle size distribution from metered dose inhalers, J. Pharm. Sci. 93 (2004) 349–363.

[34] H.D.C. Smyth, A.J. Hickey, Dynamic particle size distributions emitted from pMDIs as determined by laser diffraction: a function of time and space, in: R.N. Dalby, P.R. Byron, J. Peart, S.J. Farr (Eds.), Respiratory Drug Delivery VIII, Davis Harwood International, 2002.

[35] G. Martin, H. MacRitchie, C. Marriott, X.-M. Zeng, Characterisation of a carrier-free dry powder aerosol formulation using inertial impaction and laser diffraction, Pharm. Res. 23 (2006) 2210–2219.

[36] C. Marriott, H.B. MacRitchie, X.M. Zeng, G.P. Martin, Development of a laser diffraction method for the determination of the particle size of aerosolised powder formulations, Int. J. Pharm. 326 (2006) 39–49.

[37] X.M. Zeng, H. MacRitchie, C. Marriott, G. Martin, Correlation between inertial impaction and laser diffraction sizing data for aerosolized carrier-based dry powder formulations, Pharm. Res. 23 (2006) 2200–2209.

[38] A.H. de Boer, D. Gjaltema, P. Hagedoorn, H.W. Frijlink, Characterization of inhalation aerosols: a critical evaluation of cascade impactor analysis and laser diffraction technique, Int. J. Pharm. 249 (2002) 219–231.

[39] J. Mitchell, S. Newman, H.K. Chan, In vitro and in vitro aspects of cascade impactor tests and inhaler performance: a review, AAPS Pharm. Sci. Technol. 8 (4) (2007).

[40] B.H. Kaye, D. Alliet, L. Switzer, C. Turbitt-Daoust, The effect of shape on intermethod correlation of techniques for characterizing the size distribution of powder. Part 1. Correlating the size distribution measured by sieving, image analysis, and diffractometer methods, Particle Particle Syst Character 14 (1997) 219–224.

[41] B.H. Kaye, D. Alliet, L. Switzer, C. Turbitt-Daoust, The effect of shape on intermethod correlation of techniques for characterizing the size distribution of powder. Part 2: correlating the size distribution as measured by diffractometer methods TSI-Amherst aerosol spectrometer, and coulter counter, Particle Particle Syst Character 16 (1999) 266–272.

[42] F.M. Etzler, M.S. Sanderson, Particle size analysis: a comparative study of various methods, Particle Particle Syst Character 12 (1995) 217–224.

[43] R.N. Kelly, J. Kazanjian, Commercial reference shape standards use in the study of particle shape effect on laser diffraction particle size analysis, AAPS Pharm. Sci. Technol. 7 (2) (2006) E1–E12.

[44] A.H.L. Chow, H.H.Y. Tong, P. Chattopadhyay, B.Y. Shekunov, Particle engineering for pulmonary drug delivery, Pharm. Res. 24 (2007) 411–437.

[45] B.Y. Shekunov, J.C. Feeley, A.H.L. Chow, H.H.Y. Tong, P. York, Physical properties of supercritically-processed and micronised powders for respiratory drug delivery, KONA (2002) 178–187.

[46] D. Lu, A.J. Hickey, Liposomal dry powders as aerosols for pulmonary delivery of proteins, AAPS Pharm. Sci. Technol. 6 (4) (2005) Article 80.

[47] M. Irngartinger, V. Camuglia, M. Damm, J. Goede, H.W. Frijlink, Pulmonary delivery of therapeutic peptides via dry powder inhalation: effects of micronisation and manufacturing, Eur. J. Pharm. Biopharm. 58 (2004) 7–14.

[48] H. Steckel, N. Rasenack, P. Villax, B.W. Muller, In vitro characterization of jet-milled and in-situ-micronized fluticasone-17-propionate, Int. J. Pharm. 258 (2003) 65–75.

[49] Y.F. Maa, P.A. Nguyen, J.D. Andya, N. Dasovich, T.D. Sweeney, S.J. Shire, C.C. Hsu, Effect of spray drying and subsequent processing conditions on residual moisture content and physical/biochemical stability of protein inhalation powders, Pharm. Res. 15 (1998) 768–775.

[50] H.K. Chan, A.R. Clark, J.C. Feeley, M.C. Kuo, S.R. Lehrman, K. Pikal-Cleland, D.P. Miller, R. Vehring, D. Lechuga-Ballesteros, Physical stability of salmon calcitonin spray-dried powders for inhalation, J. Pharm. Sci. 93 (2004) 792–804.